

Interpretation of principal components of the reflectance spectra obtained from multispectral images of exposed pig brain

Kentaro Yokoyama
Motoshi Watanabe
Yohei Watanabe
Eiji Okada

Keio University
Department of Electronics and Electrical Engineering
3-14-1, Hiyoshi, Kohoku-ku
Yokohama, 223-8522, Japan
E-mail: okada@elec.keio.ac.jp

Abstract. The spatial variation in reflectance such as the blood-vessel pattern can be observed in the image of cerebral cortex. This spatial variation is mainly caused by the difference in concentrations of oxy- and deoxyhemoglobin in the tissue. We analyze the reflectance spectra obtained from multispectral images of pig cortex by principal component analysis to extract information that relates to physiological parameters such as the concentrations of oxy- and deoxyhemoglobin and physical parameters such as mean optical path length. The light propagation in a model of exposed pig cortex is predicted by Monte Carlo simulation to estimate the interpretation of physiological and physical meanings of the principal components. The spatial variance of reflectance spectra of the pig cortex can be approximately described by the first principal component. The first principal component reflects the spectrum of hemoglobin in the cortical tissue multiplied by the mean optical path length. These results imply that the wavelength dependence of mean optical path length can be experimentally estimated from the first principal component of the reflectance spectra obtained from multispectral image of cortical tissue. © 2005 Society of Photo-Optical Instrumentation Engineers. [DOI: 10.1117/1.1854671]

Keywords: brain function; multispectral imaging; principal component analysis; Monte Carlo simulation; mean optical path length.

Paper NEU-12 received Feb. 5, 2004; revised manuscript received May 1, 2004; accepted for publication Sep. 1, 2004; published online Jan. 24, 2005.

1 Introduction

The activation of the cerebral cortex induces a localized change in the volume and oxygenation of blood. The image of the activated area of the exposed cortex can be obtained by detecting the temporal change in the intensity of light at appropriate wavelengths absorbed by the cortical tissue during the activation task. The analysis of the exposed cortical image of a rat illuminated by narrow-band incident light at a 600- to 610-nm wavelength to locate the activated area was performed by Hodge et al.¹ Cannestra et al. used the optical imaging system with a narrow-band filter at a 605- to 610-nm wavelength during surgery to measure the functionally active regions in the human cortex.² The temporal change in reflectance of the exposed cortex in the visible to near-IR wavelength range primarily depends on the change in concentrations of oxyhemoglobin as well as deoxyhemoglobin in superficial cerebral regions.³⁻⁵ Differential imaging with light at a narrow-band wavelength can detect the temporal change in functional activity of the brain related to a change in the concentrations of oxy- and deoxyhemoglobin. In the differential imaging of exposed cortex, a baseline image obtained during a rest period is subtracted from the images obtained at

a task period. However, it is impossible to make the distinction between the oxy- and deoxyhemoglobin from the monochromatic images. Multiwavelength measurement of the change in reflectance of cortical tissue enables determining the change in the oxyhemoglobin concentration independently of the deoxyhemoglobin concentration.

Recently, multispectral imaging systems have been developed and applied to color image analysis in various fields such as art and natural scenes.⁶⁻⁸ The analysis of the multispectral image becomes more complicated when the number of wavelengths increases. In image data processing field, multivariate analyses, such as principal component analysis⁹ and independent component analysis, are widely used to effectively reduce the amount of information. Tsumura et al. analyzed a skin color image by independent component analysis to separate the spatial distribution of melanin and hemoglobin in skin.¹⁰ Multispectral imaging has also been applied to the exposed cortical tissue to measure the temporal change in oxy- and deoxyhemoglobin caused by the brain activation. The temporal change in oxy- and deoxyhemoglobin was calculated from the differential images at two wavelengths.¹¹ Dunn et al. simultaneously measured the cerebral blood content, oxygen saturation, and cerebral blood flow of exposed

Address all correspondence to Eiji Okada, Keio University, Department of Electronics and Electrical Engineering, 3-14-1, Hiyoshi, Kohoku-ku, Yokohama, 223-8522, Japan. Tel: +81 0 45 566 1532; Fax: +81 0 45 566 1529; E-mail: okada@elec.keio.ac.jp

cortex by combining multiwavelength imaging and laser speckle contrast imaging.¹²

The temporal change in reflectance spectra of cortical tissue depends not only on the change in concentrations of oxy- and deoxyhemoglobin but also on the mean optical path length that detected light travels in the cortical tissue. The mean optical path length is determined by the wavelength-dependent absorption and scattering coefficients. Mayhew et al. suggested that a linear spectrographic analysis method, which ignored the wavelength dependence of mean optical path length, produced unreliable results in multispectral image analysis.¹¹ However, it is difficult to experimentally obtain the wavelength dependence of the mean optical path length. The spatial variation in reflectance such as the blood-vessel pattern can be observed in the cortical image. This spatial variation is mainly caused by the difference in concentration of oxy- and deoxyhemoglobin in the cortical tissue. The spatial variation of reflectance as well as the temporal change may depend on the wavelength-dependent mean optical path length.

In this paper, we acquired the multispectral images of exposed pig cortex with a multispectral imaging system. The reflectance spectra of multispectral image of the pig cortex were analyzed by principal component analysis to extract information that relates to physiological parameters such as the concentrations of oxy- and deoxyhemoglobin and physical parameters such as the mean optical path length. The light propagation in a model of exposed pig cortex was predicted by Monte Carlo simulation to estimate the interpretation of physiological and physical meaning of the principal components of reflectance spectra of the pig cortex.

2 Background Theory

2.1 Multispectral Reflectance of Tissue

The intensity of reflected light at wavelengths λ in direction θ from exposed cortex $Y(\theta, \lambda)$ can be expressed by the dichromatic reflection model:¹³

$$Y(\theta, \lambda) = Y_s(\theta, \lambda) + Y_d(\theta, \lambda) \\ = a_s(\theta)E(\lambda) + a_d(\theta)R_d(\lambda)E(\lambda), \quad (1)$$

where $Y_s(\theta, \lambda)$ and $Y_d(\theta, \lambda)$ are the specular and diffuse reflections, respectively; $a_s(\theta)$ and $a_d(\theta)$ are the scaling factors; $R_d(\lambda)$ is the spectral reflectance for diffuse reflection; and $E(\lambda)$ is the intensity of incident light. The diffusely reflected light is strongly scattered in the biological tissue. The propagation direction of multiply scattered light tends to be independent of that of the incident light. Assuming that the angular distribution of the intensity of the diffusely reflected light is isotropic, that the specular reflection is ignored, and that the light is diffusely reflected equally in all directions, the spectral reflectance of the exposed cortex is proportional to the reflectance of diffuse reflection $R_d(\lambda)$, which can be given by

$$R_d(\lambda) = \exp[-\mu_a \langle l(\lambda) \rangle - G(\lambda)], \quad (2)$$

where μ_a is the absorption coefficient of the cortical tissue, $\langle l(\lambda) \rangle$ is the mean optical path length of the detected light traveling in the cortex, and $G(\lambda)$ is the loss due to scattering. Because the absorption of the cortical tissue is caused by sev-

eral chromophores in the tissue, the absorption coefficient can be expressed simply as the linear sum of the contribution of each chromophore.

$$R_d(\lambda) = \exp\left\{-\sum_i [c_i \epsilon_i(\lambda)] \langle l(\lambda) \rangle - G(\lambda)\right\}, \quad (3)$$

where c_i is the concentration, and ϵ_i is the molar extinction coefficient of the chromophores. In this paper, we assume that the absorption in the cortical tissue is caused by oxyhemoglobin, deoxyhemoglobin, and other chromophores.

$$-\ln[R_d(\lambda)] = c_{\text{oxy}} \epsilon_{\text{oxy}}(\lambda) \langle l(\lambda) \rangle + c_{\text{deoxy}} \epsilon_{\text{deoxy}}(\lambda) \langle l(\lambda) \rangle \\ + \mu_{a \text{ cortex}} \langle l(\lambda) \rangle + G(\lambda), \quad (4)$$

where c_{oxy} and c_{deoxy} are the concentrations of oxy- and deoxyhemoglobin; ϵ_{oxy} and ϵ_{deoxy} are the molar extinction coefficients of oxy- and deoxyhemoglobin, respectively; and $\mu_{a \text{ cortex}}$ is the absorption coefficient of the cortical tissue without hemoglobin. It is not possible to obtain the absolute concentrations of oxy- and deoxyhemoglobin from Eq. (4) because the loss by scattering $G(\lambda)$ cannot be measured from the multispectral image.

In differential imaging, the multispectral images are analyzed by pixel-by-pixel subtraction of a rest state and activated state. The temporal change in reflectance at a pixel can be given by

$$\Delta R_d(\lambda) = \ln[R_{d \text{ rest}}(\lambda)/R_{d \text{ act}}(\lambda)] \\ = \Delta c_{\text{oxy}} \epsilon_{\text{oxy}}(\lambda) \langle l(\lambda) \rangle + \Delta c_{\text{deoxy}} \epsilon_{\text{deoxy}}(\lambda) \langle l(\lambda) \rangle, \quad (5)$$

where $R_{d \text{ rest}}(\lambda)$ and $R_{d \text{ act}}(\lambda)$ are the reflectance of a cortical image obtained during a rest state and during an activated state, respectively. The absolute change in concentrations of oxy- and deoxyhemoglobin can be calculated from the change in reflectance at several wavelengths by solving a simultaneous equation derived from Eq. (5) if we obtain the mean optical path length $\langle l(\lambda) \rangle$. The mean optical path length cannot be directly measured from the multispectral images. The assumption that path length is wavelength independent has sometimes been adopted to calculate the change in concentrations of oxy- and deoxyhemoglobin, although the mean optical path length $\langle l(\lambda) \rangle$ depends on the wavelength in reality. This assumption may produce unreliable results in multispectral image analysis.

2.2 Principal Component Analysis

Principal component analysis has been used to describe original sets of data with a smaller number of uncorrelated components. Principal component analysis is an effective method to extract valuable information from a large amount of data and has been used for remote sensing, color analysis and so forth.^{14,15} In principal component analysis, the reflectance spectra are represented as a point in multidimensional vector space. A multispectral image is described as an $m \times n$ data matrix of n observations on m variables.

$$\mathbf{R} = [\mathbf{r}_1 \ \mathbf{r}_2 \ \cdots \ \mathbf{r}_n], \quad (6)$$

where \mathbf{r}_i is a spectral data in which number of wavelength is m for a pixel and n corresponds with number of pixel of the CCD camera. The first principal component gives the linear combination of the variables that gives the maximum variation. A second principal component gives the linear combination of variables that is orthogonal to the first principal component that gives the maximum variation. The goal of the principal component analysis is to find the eigenvectors of the covariance matrix.⁹ These eigenvectors correspond to the direction of the principal components of the original spectra. The variance-covariance matrix \mathbf{V} is calculated as follows:

$$\mathbf{V}_{jk} = [\mathbf{r}_j - \bar{\mathbf{r}}]^T [\mathbf{r}_k - \bar{\mathbf{r}}], \quad (7)$$

where $\bar{\mathbf{r}}$ is the average spectrum of the image. Since \mathbf{V} is symmetric matrix, a positive real number α and a nonzero vector \mathbf{u} can be found such that

$$\mathbf{V}\mathbf{u} = \alpha\mathbf{u}, \quad (8)$$

where α is an eigenvalue, and \mathbf{u} is an eigenvector of \mathbf{V} . The characteristic equation $|\mathbf{V} - \alpha\mathbf{I}| = 0$ is solved to find a nonzero \mathbf{u} . A diagonalized routine is performed to determine eigenvalues and eigenvectors of the matrix \mathbf{V} . If the matrix $\mathbf{U} = [\mathbf{u}_1 \mathbf{u}_2 \cdots \mathbf{u}_n]$ contains the eigenvectors of a matrix \mathbf{V} , then \mathbf{U} is orthogonal and \mathbf{U} can be decomposed as

$$\mathbf{V} = \mathbf{U}\mathbf{D}\mathbf{U}^T, \quad (9)$$

where \mathbf{D} is a diagonal matrix of the eigenvalues. Singular value decomposition is used for this diagonalization because of its numerical stability. These eigenvectors correspond to the directions of the principal components of the original spectra. Their statistical significance is given by their corresponding eigenvalues. The eigenvector \mathbf{u}_1 corresponding to the maximum eigenvalue α_1 indicates the direction of the first principal component. The principal components are essentially statistical value and have no physiological and physical meaning in themselves. However, the principal components for multispectral images of the cortical tissue are likely to relate to the spectra of oxy- and deoxyhemoglobin because the spatial variance in the reflectance spectra of the cortical tissue is mainly caused by the absorption of oxy- and deoxyhemoglobin.

3 Methods

3.1 Acquisition of Multispectral Image

The multispectral images of pig cortex were acquired with a multispectral imaging system. The system was installed in a stereomicroscope, as shown in Fig. 1. A surgically removed pig brain was placed under the microscope and was illuminated by a halogen lamp. The dimension of the pig brain in the median plane was about 80 mm. The surface of the cortex was kept wet with physiological saline solution. Reflected light from the cortical tissue was projected onto a cooled 16-bit CCD camera with 512×512 pixels through a filter wheel. The region of interest was around parietal region but we avoided the longitudinal fissure. The size of the field of view was about 2.3×2.3 mm. The cortical surface in the field of view was almost flat. Five narrow-band filters with the central wavelengths from 450 to 650 nm at an interval of 50 nm were

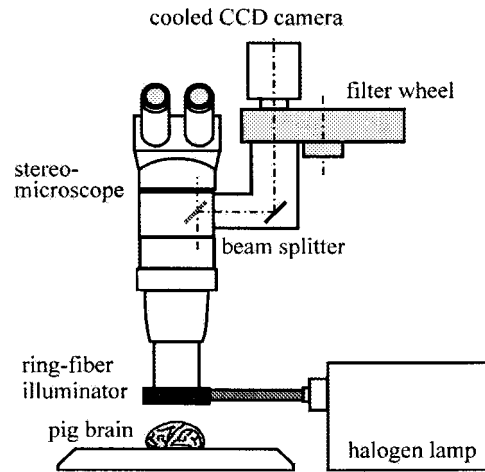


Fig. 1 Multispectral imaging system installed in a stereomicroscope.

installed in the filter wheel to acquire five spectral images of the cortical tissue. The filter wheel was controlled with a computer. The images of a diffuse-reflectance standard at each wavelength were also obtained to compensate the spectrum of the halogen lamp. The bandwidth of all the filters was 10 nm. A reflectance spectrum of cortical tissue at each pixel was extracted from the multispectral images. A set of reflectance spectra obtained from a multispectral image was analyzed by principal component analysis. The first and second principal components of six sets of multispectral images obtained from three brain samples were calculated.

3.2 Cortical Model for Image Synthesis

A cortical model was used to estimate physiological and physical interpretations of principal components for multispectral images of the exposed pig cortex. Since the surface of the exposed pig cortex in the field of view of the CCD camera was almost flat, the geometry of cortical tissue was simplified to a rectangular solid. The dimension of the model is $10 \times 10 \times 5$ mm. The model consists of $200 \times 200 \times 100$ cubic elements and each element is specified by its scattering and absorption coefficients to represent the vessel structure and tissue area, as shown in Fig. 2. The model contains six types of blood vessels with a square cross section and tissue region containing unobserved capillary bed. The hemoglobin concentration and oxygen saturation of each part of the model are shown in Table 1. The scattering and absorption coefficients of cortical tissue, and the molar extinction coefficients of oxy- and deoxyhemoglobin are shown in Figs. 3(a) and 3(b), respectively. The scattering and absorption coefficients of the cortical tissue were chosen from the reported data of pig brain.¹⁶ We used the same five wavelengths in the simulation as those used in the experiment and the spectra shown in Fig. 3 were obtained from the data at the five wavelengths by spline interpolation. The scattering coefficient is assumed to be uniform in the model and the anisotropy parameter of the model is 0.9. The absorption coefficient of each element $\mu_a(x, y, z)$ is calculated from the absorption coefficient of cortical tissue $\mu_{a, \text{cortex}}$, hemoglobin concentration $c_{\text{Hb}}(x, y, z)$, oxygen saturation $\text{SO}_2(x, y, z)$, and extinction coefficients of oxyhemoglobin ϵ_{oxy} and deoxyhemoglobin ϵ_{deoxy} as follows:

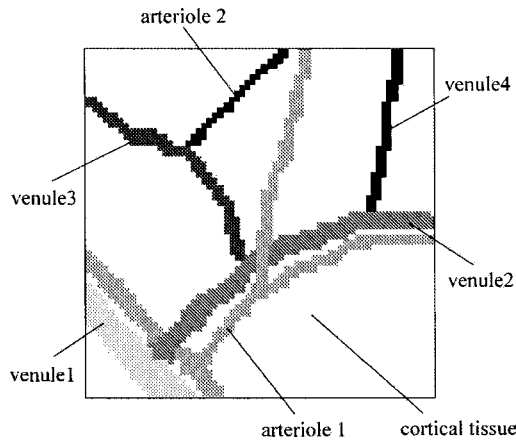


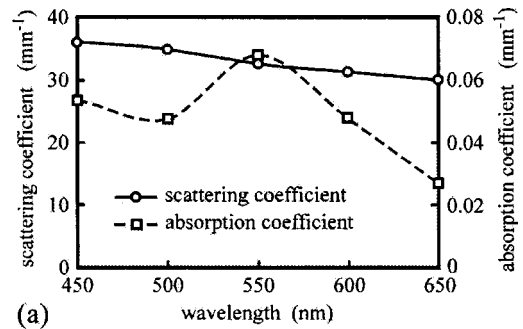
Fig. 2 Cortical tissue model for interpretation of principal component of reflectance spectra obtained from multispectral images of pig cortex. The model consists of six types of vessel and cortical tissue region containing unobserved capillary bed.

$$\begin{aligned} \mu_a(x,y,z) = & \mu_{a \text{ cortex}} + \epsilon_{\text{oxy}}c_{\text{Hb}}(x,y,z)\text{SO}_2(x,y,z) \\ & + \epsilon_{\text{deoxy}}c_{\text{Hb}}(x,y,z)[1 - \text{SO}_2(x,y,z)]. \end{aligned} \quad (10)$$

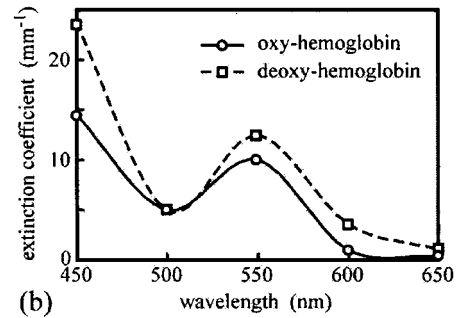
The hemoglobin concentrations of tissue and blood vessel are 93 μM and 1.86 mM, respectively. The oxygen saturation in the model ranges from 40 to 100%, as shown in Table 1. The light propagation in the model was predicted by Monte Carlo simulation based upon variance reduction algorithm.^{17,18} Photons, which had unit weight were uniformly injected into whole area of the top surface of the model to mimic parallel light. The trajectories of photons were determined by scattering coefficient and random numbers. When the photon was scattered out from the cortical surface, the photon was projected onto a CCD camera with 128×128 pixels. The size of the field of view was about 6.4×6.4 mm. The size of the pixel of the CCD camera in Monte Carlo simulation was larger than that in the experimental system to keep the computation time of the simulation within a reasonable limit. The ultimate weight of the detected photon was calculated from the absorption coefficient of each element and path length $l(\lambda)$ in which

Table 1 Hemoglobin concentration and oxygenation saturation of cortical model.

Tissue Types	Hemoglobin Concentration (mM)	Oxygen Saturation (%)
Arteriole 1	1.86	100
Arteriole 2	1.86	80
Venule 1	1.86	65
Venule 2	1.86	55
Venule 3	1.86	60
Venule 4	1.86	40
Cortical tissue	0.093	80



(a)



(b)

Fig. 3 Wavelength-dependent optical properties of the cortical model: (a) scattering and absorption coefficients of cortical tissue and (b) molar extinction coefficients of oxy- and deoxyhemoglobin. The curves were obtained from the data at the five wavelengths by spline interpolation.

the photon traveled. The internal reflection in the model caused by refractive index mismatch was considered, whereas the specular reflection of incident light was ignored. The refractive index of the model was 1.4. The ultimate weight of detected photons was accumulated with respect to each pixel of the CCD to obtain the reflectance image. Since the CCD camera with 128×128 pixels was modeled in the simulation, the 16,384 different reflectance spectra were obtained from the multispectral image of the cortical model. The reflectance spectra were analyzed by principal component analysis as well as the experimental data to obtain the first and second principal components.

The least-squares fit based on absorption factors in the cortical tissue to the first and second principal components of the reflectance spectra was performed to discuss the physiological and physical interpretation of the principal components. We assumed that the spectrum of the j 'th principal component $P_j(\lambda)$ is expressed by the linear function of the spectrum of an absorption factor:

$$P_j(\lambda) = kF_i(\lambda) + \delta(\lambda), \quad (11)$$

where $F_i(\lambda)$ is the spectrum of an absorption factor i , and $\delta(\lambda)$ is residual component. The absorption spectra of oxyhemoglobin, deoxyhemoglobin, cortical tissue, 80% oxygenated hemoglobin, and 80% oxygenated hemoglobin multiplied by mean optical path length were chosen as the absorption factors. The coefficient k was calculated by the least-squares fitting method. The sum of squares of the residual components at the five wavelengths for the five absorption factors was

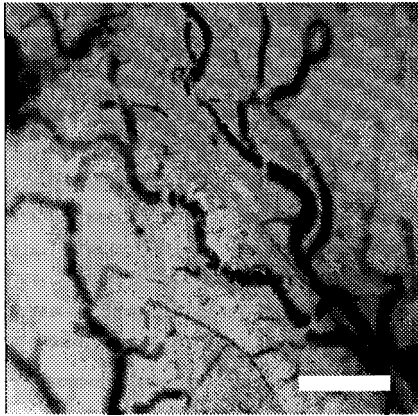


Fig. 4 Image of pig cortex at a 550-nm wavelength acquired with the multispectral imaging system. The bar indicates 500 μm .

calculated to evaluate the similarities of wavelength dependence of the principal components to those of the absorption factors.

4 Results

An image of a surgically removed pig brain obtained with a 550-nm filter is shown in Fig. 4. Although the cortical tissue has no blood circulation, a blood-vessel pattern, which is caused by the difference in hemoglobin concentrations, can be clearly observed in the image. Figure 5 shows typical 24 reflectance spectra at cortical tissue and at various blood vessels obtained from the multispectral images at five wavelengths. The reflectance data at five wavelengths detected with each pixel of the CCD camera were connected by spline interpolation to obtain the spectrum. The reflectance spectra of the pig cortex vary from position to position. The first and second principal components obtained from the reflectance spectra of the pig cortex detected with all the pixel of the CCD camera are shown in Fig. 6. The result is average of six sets of multispectral images and the bars in the figure represent standard deviation. The standard deviation of the first principal component is much smaller than that of the second principal component. This indicates that the first principal component of the reflectance spectra is less influenced by individual specificity of the cortical tissue and noise. The percentages of variance

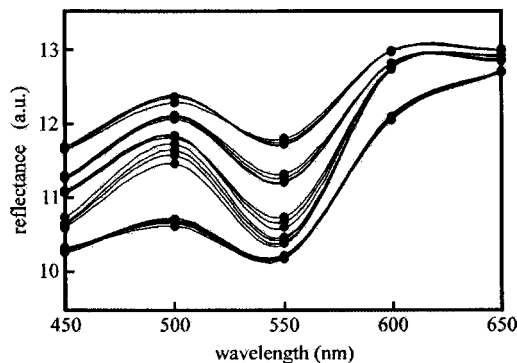


Fig. 5 Typical reflectance spectra obtained from multispectral images of exposed pig cortex. The curves were obtained from the measured reflectance at the five wavelengths by spline interpolation.

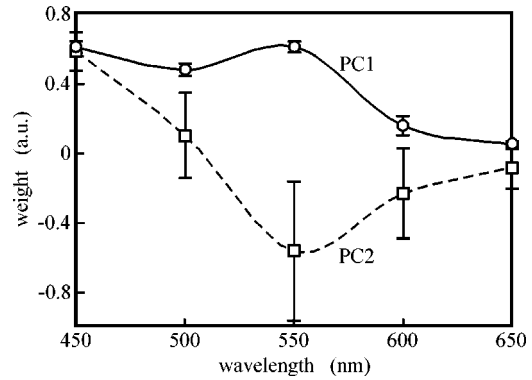


Fig. 6 First and second principal components of reflectance spectra obtained from six sets of multispectral images of pig cortex. The curves were obtained from the weight calculated from multispectral images at the five wavelengths by spline interpolation.

accounted for by the first and second principal components were 87.3 ± 4.9 and $4.12 \pm 5.0\%$, respectively. The variance in the reflectance spectra of the pig cortex is mainly concentrated in the first principal component.

The propagation of light at five wavelengths in the cortical model shown in Fig. 2 was predicted by Monte Carlo simulation to calculate the reflectance spectra and mean optical path length of light detected with each pixel of the CCD. Ten million photons were injected to calculate the results as each wavelength. Since the results calculated with ten million photons were almost the same as those with eight million photons, the statistical error of Monte Carlo simulation in the results can be negligible. The wavelength-dependent mean optical path length for the cortical model is shown in Fig. 7. The mean optical path length steeply increases when wavelength is longer than 600 nm. The mean optical path length at 650 nm wavelength is about five times longer than that at 550 nm. Typical reflectance spectra of the cortical model are shown in Fig. 8. Two valleys of spectra at 450 and 550 nm, which relate to the absorption peaks of cortical tissue and hemoglobin, can be observed in all the spectra. This tendency of the spectral peaks of the cortical model is similar to that of the experimentally measured reflectance spectra of pig cortex shown in Fig. 5. The first and second principal components

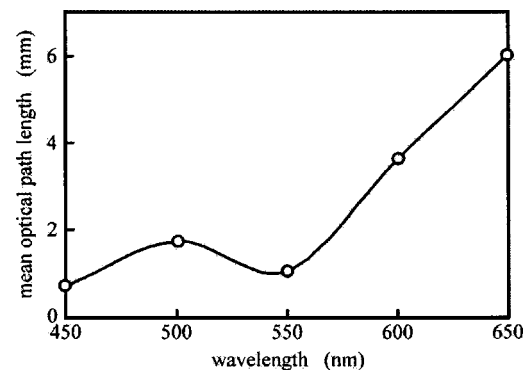


Fig. 7 Wavelength-dependent mean optical path length of the detected photons traveling in the cortical model predicted by Monte Carlo simulation. The curve was obtained from the mean optical path length predicted at the five wavelengths by spline interpolation.

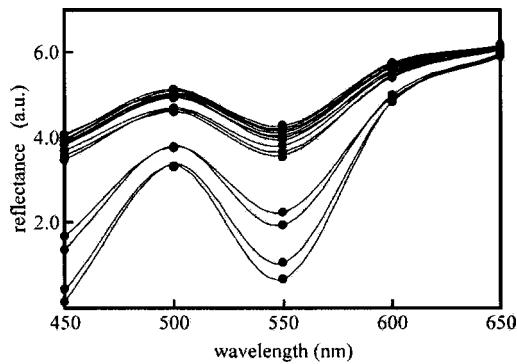


Fig. 8 Typical reflectance spectra obtained from multispectral images of the cortical model predicted by Monte Carlo simulation. The curves were obtained from the reflectance predicted at the five wavelengths by spline interpolation.

calculated from the reflectance spectra obtained from the multispectral image of the cortical model are shown in Fig. 9. The percentages of variance accounted for by the first and second principal components were 96.7 and 1.7%, respectively. The variance in the reflectance spectra of the cortical model can be almost described by the first principal component. The first principal component of the reflectance spectra of the cortical model is highly similar to that of the pig cortex shown in Fig. 6, whereas the second principal component does not agree with that of the experimental result. These results indicate that the first principal component of the pig cortex is reflected in hemoglobin concentration and oxygen saturation because the variation in reflectance spectra of the cortical model is caused by the concentrations of oxy- and deoxyhemoglobin. The second principal component of the reflectance spectra of the pig brain may not imply any parameters corresponding to the concentrations of oxy- and deoxyhemoglobin. The large deviation of the second principal component of the experimental data implies that the influence of noise in the reflectance spectra on the second principal component is greater than that on the first principal component. The reflectance spectra of the cortical model of which the hemoglobin concentration of blood vessels was 0.19 mM but the vessel structure was the same was

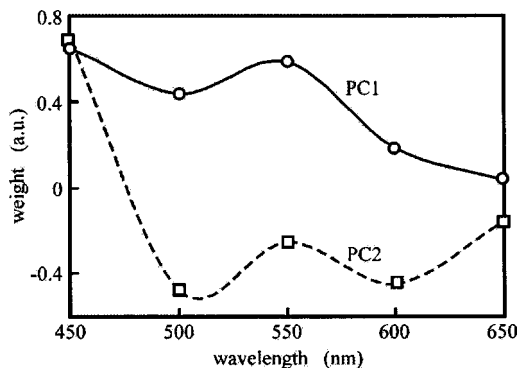


Fig. 9 First and second principal components of reflectance spectra obtained from multispectral images of the cortical model predicted by Monte Carlo simulation. The curves were obtained from the weight calculated from multispectral images at the five wavelengths by spline interpolation.

Table 2 Sum of squares residuals of least-squares fit based on absorption factors.

Absorption Factors	Sum of Squares of Residuals	
	PC 1	PC 2
Oxyhemoglobin	0.074	0.930
Deoxyhemoglobin	0.135	0.884
Cortical tissue	0.122	0.935
80% oxygenated hemoglobin	0.085	0.918
80% oxygenated hemoglobin × mean optical path length	0.006	0.997

also predicted by Monte Carlo simulation. Although the percentage of variance accounted for by the first principal component was reduced to 87.1%, the wavelength dependence of the first principal component of the reflectance spectra is almost the same as that shown in Fig. 8.

A linear least-squares fit to the first and second principal components of the reflectance spectra of the cortical model based on absorption factors in the cortical tissue was performed to determine interpretations of the principal components. The factors are spectra of oxyhemoglobin, deoxyhemoglobin, cortical tissue of pig, 80% oxygenated hemoglobin, and 80% oxygenated hemoglobin multiplied by the mean optical path length shown in Fig. 7. The oxygen saturation of the hemoglobin for the least-squares fit is the same as that in the cortical model. The sum of squares of residuals of the least-squares fit based on each absorption factor are listed in Table 2. The residual for the spectrum of 80% oxygenated hemoglobin multiplied by the mean optical path length is significantly smaller than that of other absorption factors. The dotted lines in Fig. 10 show the curves of least-squares fit to the first principal component of the reflectance spectra of the cortical

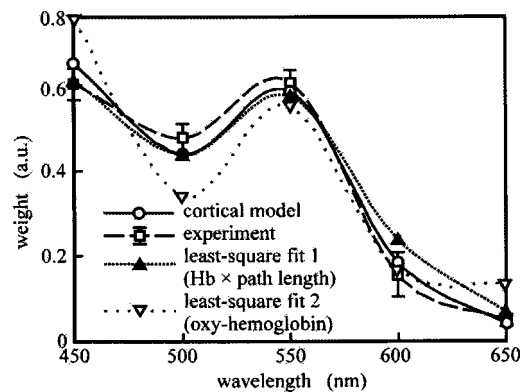


Fig. 10 Linear least-squares fit to the first principal component of reflectance spectra obtained from multispectral images of the cortical model based on absorption spectrum of 80% oxygenated hemoglobin multiplied by mean optical path length and based on absorption spectrum of oxyhemoglobin. The first principal component of reflectance spectra obtained from six sets of multispectral images of pig cortex is also shown. The curves were obtained from the weight calculated at the five wavelengths by spline interpolation.

model based on the spectrum of 80% oxygenated hemoglobin multiplied by the mean optical path length and based on the spectrum of oxyhemoglobin. The first principal components of both the cortical model (solid line) and the pig cortex (broken line) are also shown in the figure. The curve of the least-squares fit based on the spectrum of the hemoglobin multiplied by the mean optical path length well approximates the first principal components of the reflectance spectra of both the cortical model and the real pig cortex.

5 Discussion

Principal component analysis can extract meaningful information from multispectral images. The first principal component for the cortical model agrees well with that for the real pig cortex, whereas the second principal component for the cortical model is different from that for the real cortex. Although the reflectance spectra of real pig cortex are influenced by variety of factors, the concentrations of oxy- and deoxyhemoglobin was changed only in the cortical model. Modeling light propagation in cortical tissue is not enough to describe the phenomena corresponding to the second principal component for the real cortical tissue. However, the percentages of variance accounted for by the first principal components for experimental data is almost 90% and the individual difference in the second principal component is much greater than that in the first principal component. These results indicate that the variance of the reflectance spectra of the pig cortex can be approximately described by the first principal component.

The linear least-squares fit to the principal components of the reflectance spectra of the cortical model based on absorption factors in the cortical tissue reveals that the first principal component strongly correlates with the spectrum of hemoglobin in the cortical tissue multiplied by the mean optical path length. Note that the first principal component of the reflectance spectra of the pig cortex measured with the multispectral imaging system approximates the wavelength dependence of the hemoglobin absorption multiplied by the mean optical path length. This implies that the wavelength dependence of the mean optical path length can be estimated from the first principal component of the reflectance spectra of the cortical tissue if the spectrum of hemoglobin in the cortical tissue can be obtained. Although the spectrum of hemoglobin varies with oxygen saturation, the difference is not significant in a case where the oxygen saturation of the cortical tissue remains within normal limits. Note that it is impossible to calculate the absolute optical path length from the first principal components because principal components do not directly relate to any physiological and physical parameters.

In the differential imaging measurement, the mean optical path length is required to calculate the change in concentrations of oxy- and deoxyhemoglobin. The mean optical path length strongly depends on wavelength, as shown in Fig. 7. It is suggested that a linear spectrographic analysis method, which ignores wavelength-dependent path length, produces unreliable results.⁹ Although the path length scaling analysis can improve the differential imaging measurement, it is difficult to experimentally obtain the wavelength dependence of mean optical path length. The estimation of the wavelength dependence of the mean optical path length in cortical tissue from the first principal component can be helpful for the path

length scaling analysis even if the estimated path length is a relative quantity.

In future work, we plan to apply the proposed path length estimation from the first principal component to the multispectral imaging of the exposed cortical tissue of small animals such as rats. Since the brain of the rat is smaller than that of the pig, we should examine the influence of specular reflection from the curved cortical surface on the first principal component of multispectral image. We should also examine the influence of diameter distribution of blood vessels on the first principal component. The mean optical path length of diffusely reflected light depends on the absorption coefficient of the cortical tissue as well as the scattering coefficient. The difference in mean optical path length in various part of tissue caused by the absorption coefficient cannot be neglected if the differences in absorption coefficient of tissue are significant. The mean optical path length of light reflected at a large vessel may be different from that reflected at the cortical tissue containing an unobserved capillary bed. It is better to avoid using the spectrum of reflectance at large blood vessels to estimate the wavelength dependence of the mean optical path length in the cortical tissue by principal component analysis.

6 Conclusions

In this paper, the reflectance spectra obtained from multispectral images of the pig cortex were analyzed by principal component analysis. The spatial variance of reflectance spectra of the pig cortex can be approximately described by the first principal component. The light propagation in the cortical model was predicted by Monte Carlo simulation to estimate the physiological and physical interpretation of the principal components. The first principal component for the cortical model agrees well with that for the pig cortex and it reflects the spectrum of hemoglobin in the cortical tissue multiplied by the mean optical path length. These results imply that the wavelength dependence of the mean optical path length in cortex can be experimentally estimated from the first principal component of the reflectance spectra obtained from multispectral image of the exposed cortical tissue.

Acknowledgments

The authors wish to thank Mr. K. Honjyo at Keio University, Dr. A. Maki at Hitachi Co. Ltd., Prof. Y. Yamada at the University of Electro-Communications, and Dr. H. Iseki at Tokyo Women's Medical University for their contributions to this work. This work was partly supported by the Japan Society for the Promotion of Science, Grants-in-Aid for Scientific Research No. 13558116, and Grant-in-Aid for the 21st Century Center of Excellence for Optical and Electronic Device Technology for Access Network from the Ministry of Education, Culture, Sport, Science, and Technology in Japan.

References

1. C. J. Hodge, Jr., R. T. Stevens, H. Newman, J. Merola, and C. Chu, "Identification of functioning cortex using cortical optical imaging," *Neurosurgery* **41**, 1137–1145 (1997).
2. A. F. Cannestra, S. Y. Bookheimer, N. Pouratian, A. O'Farrell, N. Sicotte, N. A. Martin, D. Becker, G. Rubino, and A. W. Toga, "Temporal and topographical characterization of language cortices using intraoperative optical intrinsic signals," *Neuroimage* **12**, 41–54 (2000).

3. B. C. Wilson, E. M. Sevick, M. S. Patterson, and B. Chance, "Time-dependent optical spectroscopy for biomedical applications," *Proc. IEEE* **80**, 918–930 (1992).
4. C. E. Elwell, H. Owen-Reece, J. S. Wyatt, M. Cope, E. O. R. Reynolds, and D. T. Delpy, "Influence of respiration and changes in expiratory pressure on cerebral haemoglobin concentration measured by near infrared spectroscopy," *J. Cereb. Blood Flow Metab.* **16**, 353–357 (1996).
5. A. Maki, Y. Yamashita, Y. Ito, E. Watanabe, Y. Mayanagi, and H. Koizumi, "Spatial and temporal analysis of human motor activity using noninvasive NIR topography," *Med. Phys.* **22**, 1997–2005 (1995).
6. S. Tominaga, "Spectral imaging by a multi-channel camera," *J. Electron. Imaging* **8**, 332–341 (1999).
7. S. Baronti, A. Casini, F. Lotti, and S. Porcinai, "Multispectral imaging system for the mapping of pigments in works of art by use of PCA," *Appl. Opt.* **37**, 1299–1309 (1998).
8. C.-C. Chiao, T. W. Cronin, and D. Osorio, "Color signals in natural scenes: characteristics of reflectance spectra and effects of natural illuminants," *J. Opt. Soc. Am. A* **17**, 218–224 (2000).
9. A. Basilevsky, *Statistical Factor Analysis and Related Methods: Theory and Applications*, Wiley, New York (1994).
10. N. Tsumura, H. Haneishi, and Y. Miyake, "Independent-component analysis of skin color image," *J. Opt. Soc. Am. A* **16**, 2169–2176 (1994).
11. J. Mayhew, Y. Zheng, Y. Hou, B. Vuksanovic, J. Berwick, S. Askew, and P. Coffey, "Spectroscopic analysis of changes in remitted illumination: the response to increased neural activity in brain," *Neuroimage* **10**, 304–326 (1999).
12. A. K. Dunn, A. Devor, H. Bolay, M. L. Andermann, M. A. Moskowitz, A. M. Dale, and D. A. Boas, "Simultaneous imaging of total cerebral hemoglobin concentration, oxygenation, and blood flow during functional activation," *Opt. Lett.* **28**, 28–30 (2003).
13. S. A. Shafer, "Using color to separate reflection components," *Coor. Res. Appl.* **10**, 210–218 (1985).
14. J. P. S. Parkkinen, J. Hallikainen, and T. Jaaskelainen, "Characteristic spectra of Munsell colors," *J. Opt. Soc. Am. A* **6**, 318–322 (1989).
15. P. J. Ready and P. A. Wintz, "Information extraction, SNR improvement, and data compression in multispectral image," *IEEE Trans. Commun.* **COM21**, 1123–1131 (1973).
16. P. van der Zee, "Measurement and modelling of the optical properties of human tissue in the near infrared," PhD Thesis, University of London (1993).
17. B. C. Wilson, "A Monte Carlo model for the absorption and flux distribution of light in tissue," *Med. Phys.* **10**, 824–830 (1983).
18. P. van der Zee and D. T. Delpy, "Simulation of the point spread function for light in tissue by a Monte Carlo technique," *Adv. Exp. Med. Biol.* **215**, 179–191 (1987).